Journal of Materials Chemistry C

ROYAL SOCIETY OF CHEMISTRY

PAPER

View Article Online
View Journal | View Issue

Cite this: J. Mater. Chem. C, 2022, 10, 2800

Low nonradiative energy losses within 0.2 eV in efficient non-fullerene all-small-molecule organic solar cells†

Ziyun Huang,‡[abcd] Yanan Shi,‡[ab] Yilin Chang,[ab] Chen Yang,[ab] Min Lv,[ab] Yifan Shen,[abc] Yanan Liu,[ae] Jianqi Zhang,[a] Kun Lu *[ab] and Zhixiang Wei[ab]

Despite the remarkable progress achieved in the field of non-fullerene acceptor (NFA)-based organic photovoltaics (OPVs) in recent years, the large energy loss remains a major factor limiting the power conversion efficiency (PCE) of OPVs. Although many studies on polymer OPVs have been reported, low energy loss systems with high efficiency are rarely reported with all-small-molecule organic-solar-cells (ASM-OSCs). This is partially because a low energetic offset between donors and acceptors is usually required to have a small energy loss, which could result in an insufficient exciton dissociation driving force, making the trade-off between the device performance and energy loss an important research focus. In this article, we report ASM-OSCs based on three small molecule donors ZR1-C2, ZR1-C3 and ZR1-C4 with small molecule NFAs BTP-C11-N2Cl, BTP-C9-N2F and BTP-C9-N4F. Charge carrier mobilities, exciton dissociation efficiency and charge collection efficiency were measured and calculated for blends ZR1-C3:TP-C11-N4Cl, ZR1-C3:BTP-C9-N2F and ZR1-C3:BTP-C9-N4F, revealing good charge transport properties. Morphology characterization methods such as AFM, TEM and GIWAXS have been employed, demonstrating excellent molecular compatibility and suitable phase separation with fibrous structures that provides efficient charge transport channels. By morphology and charge carrier optimization, the highest PCE of 14.29% was achieved with a small nonradiative energy loss of 0.2 eV which, to the best of our knowledge, is the highest PCE value for ASM-OSCs with a non-radiative voltage loss $\leq$ 0.2 eV, reaching a balance between high performance and low energy loss.

Received 8th September 2021,
Accepted 15th November 2021

DOI: 10.1039/d1tc04264e

rsc.li/materials-c

Introduction

Organic solar cells (OSCs) have been widely investigated and remarkable progress has been achieved in recent years, as they offer several advantages such as flexibility, light weight and low-cost fabrication.[1–7] In the past 5 years, non-fullerene acceptor (NFA)-based organic photovoltaic devices (OPVs) have received extensive attention and pushed the power conversion efficiency (PCE) of single-junction OSCs to over 18% with polymer donors.[8–13] Compared with polymers, small molecules have intrinsic advantages such as a definite chemical structure, easy purification process, and little batch-to-batch variation.[14–16] A PCE of over 15% has been reported for all-small-molecule organic solar cells (ASM-OSCs), making them more promising toward commercialization, and have received massive attention recently.[14,17–22] Although breakthroughs have been made, further improvement on the PCE of OSCs still remains a challenge, and large energy loss is considered a major factor limiting the PCE of OPVs. Many studies related to energy loss in polymer OPVs have been discussed,[23–28] but low energy loss systems with high efficiency are rarely reported in ASM-OSCs. This is partially because low energetic offset between donors and acceptors is usually required to obtain small energy loss, which could result in an insufficient exciton dissociation driving force that leads to small current.[27] Although efficient charge separation under low driving forces has been reported in several polymer systems,[29,30] we believe that ASM-OSCs also have prospective potency for energy loss optimization. Previous research studies have shown that the open-circuit voltage (V_{OC}) is usually proportional to the difference between the highest occupied molecular orbital (HOMO) of the donor and the

[a] CAS key laboratory of nanosystem and hierarchical fabrication, CAS Center for Excellence in Nanoscience, National Center for Nanoscience and Technology, 100190 Beijing, China. E-mail: lvk@nanoctr.cn
[b] University of Chinese Academy of Sciences, 100049 Beijing, China
[c] Sino-Danish Center for Education and Research, Sino-Danish College, University of Chinese Academy of Sciences, 100190 Beijing, China
[d] Interdisciplinary Nanoscience Center (iNANO), Aarhus University, Denmark
[e] Tianjin Key Laboratory of Molecular Optoelectronic Sciences, Department of Chemistry, School of Science, Tianjin University, Tianjin 300072, China

† Electronic supplementary information (ESI) available. See DOI: 10.1039/d1tc04264e

‡ These authors contributed equally to this work.

lowest unoccupied molecular orbital (LUMO) of the acceptor. Taking acceptor Y6 as an example, the famous polymer donor PM6, with the HOMO energy level of −5.53 eV, exhibits a V_{OC} of 0.835 when blended with Y6,[31] while small molecule donor ZR1, with a higher HOMO of −5.32 eV, was reported to give a higher V_{OC} of 0.861 eV,[32] which conflicts with the previous empirical conclusion. Since energy loss is approximately the difference between the band-gap and V_{OC} of the blend, small molecule donors may possess the potential to reach lower energy loss under a similar energetic offset when compared with polymers.

In previous studies, adjusting the alkyl-chain branching position has been proposed as an efficient strategy to improve the photovoltaic performances of solar cells by controlling the crystallinity and molecular miscibility.[33] In 2019, small molecule donor ZR1 was designed and reported, achieving a high efficiency of 14.34% with Y6.[32] In 2020, Zhou *et al.* reported a series of donors ZR2-C1, ZR2-C2 and ZR2-C3, where the butyl and hexyl of ZR1 on the side-chain end groups were substituted with hexyl and octyl. By systematically moving the branching point away from the core moiety, the power conversion efficiencies of their blends were increased from 11.79% to 14.78%, with a simultaneous improvement in both FF and short circuit current (J_{SC}). End group modulation is another popular method to tune the energy bandgaps and regulate the molecular aggregations in small molecule acceptors.[34–37] Recently, an extended end group from the 2-(3-oxo-2,3-dihydro-1*H*-inden-1-ylidene)malononitrile (IC) to the 2-(3-oxo-2,3-dihydro-1*H*-cyclopenta[*b*] naphthalen-1-ylidene)malononitrile (NINCN) has been reported and an excellent result has been achieved in polymer OSCs.[23] The enlarged conjugated area of the end group could enhance the molecular interaction and increase the HOMO–LUMO energy levels of acceptors,[23,35,37] reducing the HOMO offset between the donor and acceptor materials, so that voltage loss is reduced and a high V_{OC} is obtained.

In this study, based on the previously reported ZR1 and the strategy of alkyl-chain branching point modulation, we designed and synthesized small molecule donors ZR1-C2, ZR1-C3 and ZR1-C4, the molecular structures of which are shown in Fig. 1, and the photovoltaic parameters with acceptor Y6 are listed in Table S1 (ESI†). The highest efficiency of 15.12% has been achieved by ZR1-C3, with significant improvement in FF when compared with ZR1. Then, dithienothiophen[3,2-*b*]-pyrrolobenzothiadiazole (BTP)-based non-fullerene acceptor (NFA) with different halogen substitution were designed and synthesized, among which BTP-C9-N2Cl, BTP-C9-N2Cl and BTP-C11-N4Cl were shifted out for their poor solubility in chloroform. The remaining acceptors BTP-C11-N2Cl, BTP-C9-N2F and BTP-C9-N4F were then blended with ZR1-C3 to form ASM-OSCs. The molecular structures of the donor and acceptors are shown in Fig. 1a. The non-radiative voltage loss of all these three systems is $\leq$ 0.2 eV, which is rarely reported by ASM-OSCs and is almost near to those of inorganic solar cells based on Si.[38] The optimized device based on ZR1-C3 as the donor and BTP-C9-N4F as the acceptor gave an excellent PCE of 14.29%, which, to the best of our knowledge, is the highest PCE

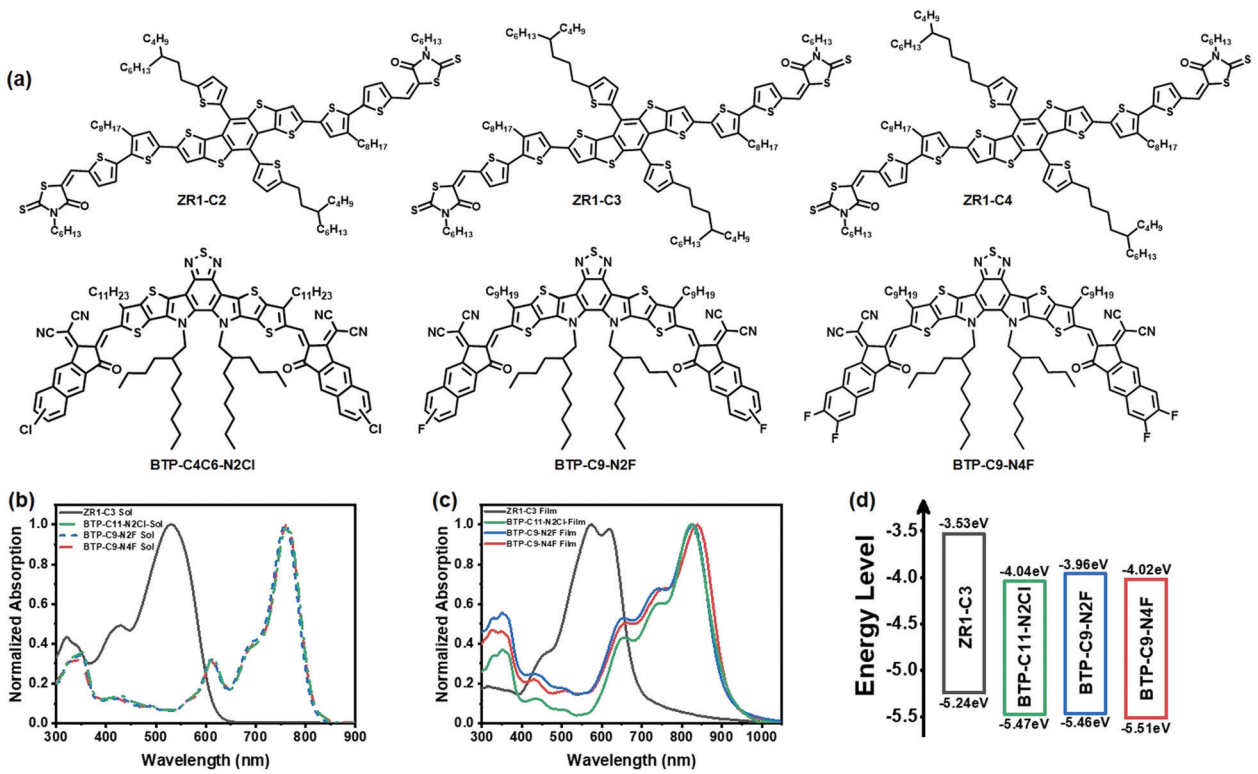

Fig. 1 Molecular structures (a), normalized solution absorption spectrum (b), normalized film absorption spectrum (c) and energy levels (d) of ZR1-C3, BTP-C11-N2Cl, BTP-C9-N2F and BTP-C9-N4F.

value for ASM-OSCs with a non-radiative voltage loss $\leq$ 0.2 eV, achieving high PCE and high non-radiative voltage loss simultaneously.

Results and discussion

In this study, the conventional structure of glass/ITO/PEDOT:PSS/active layer/PFN-Br/Ag was fabricated for all devices to investigate their photovoltaic performance. The molecular structures are shown in Fig. 1a and the optimized photovoltaic parameters are listed in Table 1. The 2-(3-oxo-2,3-dihydro-1H-cyclopenta[*b*] naphthalen-1-ylidene) malononitrile (NINCN) end group of acceptors enabled a high LUMO energy level, and thus a V_{OC} as high as 0.90 V was obtained from ZR1-C3: BTP-C9-N2F and ZR1-C3: BTP-C11-N2Cl systems, which is higher than most of BTP-based non-fullerene small-molecule acceptors. By further increasing the substituted fluorine atoms on the end groups, a simultaneous increase in both J_{SC} and FF appears with a small decrease in V_{OC}, leading to an increase in efficiency from slightly above 11% to 14.29% in the ZR1-C3:BTP-C9-N4F system.

The current density–voltage (*J–V*) characteristics and external quantum efficiency (EQE) curves are plotted in Fig. 2. The calculated J_{SC} from the EQE spectrum is 19.83 mA cm^{-2}, 19.70 mA cm^{-2} and 22.86 mA cm^{-2} for ZR1-C3:BTP-C11-N2Cl, ZR1-C3:BTP-C9-N2F and ZR1-C3:BTP-C9-N4F, respectively, which is consistent with the values obtained from *J–V* curves (error within 5%). The shape of the EQE curves is almost identical, with ZR1-C3:BTP-C9-N4F exhibiting overall higher efficiency in the range of 450 to 1000 nm, indicating better light utilization and management. The charge carrier mobility of each device was determined by the space charge-limited current (SCLC) and is plotted in Fig. S1a and b (ESI†). The electron mobility was detected using the device architecture of glass/ITO/ZnO/active layer/PFN-Br/Al, while the hole mobility was determined using the glass/ITO/PEDOT:PSS/active layer/MoO_X/Ag device structure. The electron/hole mobilities of devices with ZR1-C3:BTP-C11-N2Cl, ZR1-C3:BTP-C9-N2F and ZR1-C3:BTP-C9-N4F as active layers were calculated to be 4.21×10^{-4} cm^2 V^{-1} s^{-1}/1.48×10^{-4} cm^2 V^{-1} s^{-1}, 6.68×10^{-4} cm^2 V^{-1} s^{-1}/5.33×10^{-4} cm^2 V^{-1} s^{-1}, and 7.68×10^{-4} cm^2 V^{-1} s^{-1}/7.57×10^{-4} cm^2 V^{-1} s^{-1}, respectively. An overall higher carrier mobility and better balanced electron/hole mobility ratio (1.01) were achieved by ZR1-C3:BTP-C9-N4F when compared with others, providing better charge transport properties that led to a simultaneous increase in both J_{SC} and FF.[39,40]

To further investigate the light absorption and exciton dissociation process, the dependences of photocurrent density

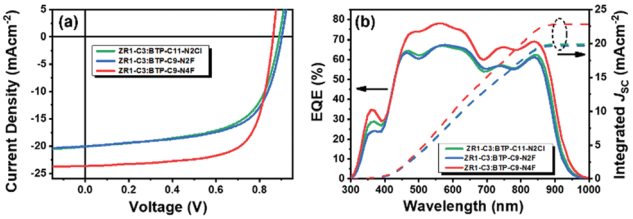

Fig. 2 The current density–voltage characteristics (a) and the corresponding external quantum efficiency (EQE) spectrum (b) of the optimized devices. The solid line represents the EQE curve and the dashed line represents the integrated J_{SC} by EQE.

(J_{ph}) on the effective voltage (V_{eff}) were measured and are plotted in Fig. S1c (ESI†). When the effective voltage is large enough (*i.e.*, $V_{eff} \geq 2$ V), all photo-generated excitons are dissociated and J_{ph} reaches saturation and is defined as J_{sat}. The J_{sat} is 21.80 mA cm^{-2} for the ZR1-C3:BTP-C11-N2Cl system, 20.80 mA cm^{-2} for the ZR1-C3:BTP-C9-N2F system and 23.99 mA cm^{-2} for the ZR1-C3:BTP-C9-N4F system, which is consistent with the measured J_{SC}. Moreover, exciton dissociation efficiency (η_{diss}) and charge collection efficiency (η_{coll}) were obtained by calculating the ratio of J_{ph}/J_{sat}. Under short-circuit conditions, η_{diss} was calculated to be 92.04% for the ZR1-C3:BTP-C11-N2Cl system, 95.81% for the ZR1-C3:BTP-C9-N2F system and 98.29% for the ZR1-C3:BTP-C9-N4F system, while under maximum power conditions, η_{coll} was calculated to be 78.36% for the ZR1-C3:BTP-C11-N2Cl system, 69.31% for the ZR1-C3:BTP-C9-N2F system and 83.21% for the ZR1-C3:BTP-C9-N4F system. The blend with BTP-C9-N4F as the acceptor exhibited the highest exciton dissociation rate as well as charge collecting efficiency among them, explaining its high FF and J_{SC}.

The surface morphology analysis of the active layers was conducted by atomic force microscopy (AFM), as shown in Fig. 3(a–c). The root mean-square (RMS) roughness is calculated to be 1.79, 1.51 and 1.65 for ZR1-C3:BTP-C11-N2Cl, ZR1-C3:BTP-C9-N2F and ZR1-C3:BTP-C9-N4F blends, respectively. Fairly low RMS values are obtained by all devices, indicating a smooth surface with nice molecular compatibility between the donor and acceptors. Relatively smaller domains were observed by the ZR1-C3:BTP-C9-N4F blend, which can avoid over-aggregation of the donor or acceptor.[41,42] To gain more in-depth insight into the bulk morphology and phase distribution, transmission electronic microscopy (TEM) was conducted and is shown in Fig. 3(d–f). Clear fibrous structures are observed in all three blends, forming an efficient charge transport channel that supports high J_{SC} and FF.[43,44] One thing worth noticing is that a clear ring can be observed in the selected area electron

Table 1 Optimized photovoltaic parameters of devices under the illumination of AM 1.5G, 100 mW cm^{-2}. The average efficiencies were calculated based on 10 cells prepared from different batches

Active layers	V_{OC} (V)	J_{SC} (mA cm^{-2})	FF (%)	PCE (%)
ZR1-C3:BTP-C11-N2Cl	0.89 (0.88 ± 0.01)	20.06 (20.03 ± 0.85)	61.23 (60.03 ± 1.20)	11.01 (10.71 ± 0.30)
ZR1-C3:BTP-C9-N2F	0.90 (0.89 ± 0.01)	20.02 (19.96 ± 0.70)	62.89 (61.48 ± 1.41)	11.44 (11.01 ± 0.43)
ZR1-C3:BTP-C9-N4F	0.86 (0.85 ± 0.01)	23.63 (23.61 ± 0.37)	69.75 (69.50 ± 0.88)	14.29 (14.02 ± 0.27)

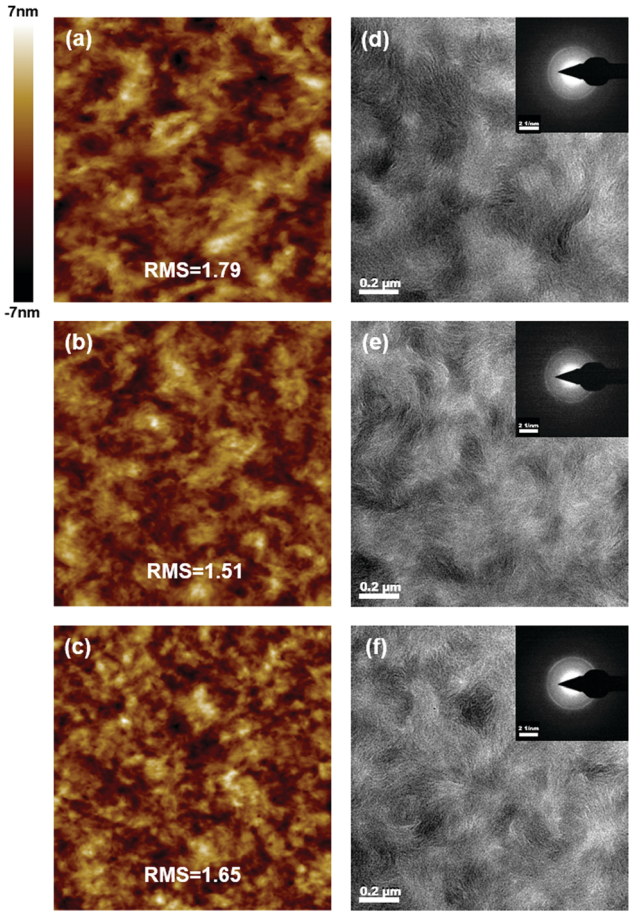

Fig. 3 AFM and TEM images of (a and d) ZR1-C3:BTP-C11-N2Cl, (b and e) ZR1-C3:BTP-C9-N2F and (c and f) ZR1-C3:BTP-C9-N4F. The scale bars of TEM images are 200 nm. The insets show the selected area electron diffraction (SAED) patterns of the blends.

diffraction (SAED) pattern shown in the inset of Fig. 3(d–f), which is rarely reported in ASM-OSCs and indicates good crystallinity. The diffraction signal is located at a distance of 0.357 nm for all three blends, corresponding to the (010) π–π stacking distance of ZR1-C3.[45] This phenomenon further supports that the fibrous structure originates from the self-assembly of donor molecule ZR1-C3. Consistent with the AFM morphology, the ZR1-C3:BTP-C9-N4F blend formed an interconnected network structure with a smaller-sized domain, which can give more donor/acceptor interfaces that reduce the electron–hole recombination, leading to sufficient exciton separation.[41,46] This is also consistent with previously calculated results.

To investigate the molecular packing and orientation of pristine films (Fig. S2, ESI†) as well as blend active layers (Fig. 4), two-dimensional grazing-incident wide-angle X-ray scattering (2D GIWAXS) was conducted. The d-spacing and crystal coherence length (CCL) values of (100) and (010) are listed in Table S2 (ESI†). The pristine donor ZR1-C3 film showed strong crystallinity with an edge-on orientation, whereas three acceptors showed a clear face-on orientation with similar weak crystallinity. In the blend films, the

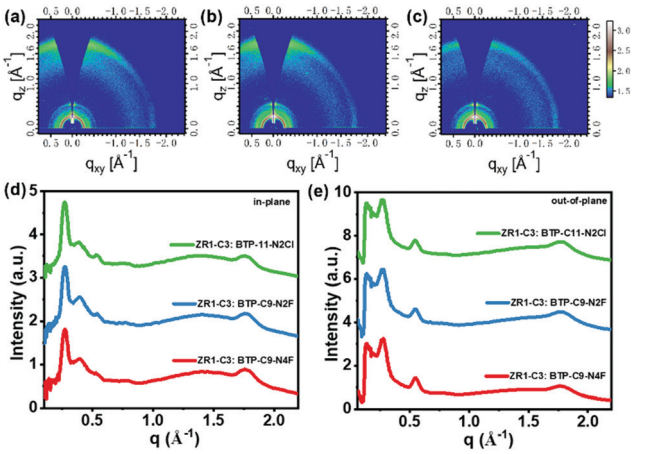

Fig. 4 GIWAXS patterns of (a) ZR1-C3:BTP-C11-N2Cl, (b) ZR1-C3:BTP-C9-N2F and (c) ZR1-C3:BTP-C9-N4F. (d) In-plane and (e) out-of-plane line cuts of the corresponding GIWAXS pattern.

crystallinity of the donor was greatly affected by the addition of small molecule acceptors, as is shown in Fig. S3 (ESI†). After thermal annealing, an obvious increase in the crystallinity of both donors and acceptors can be observed, as evidenced by the appearance and narrowing of both (100) and (010) peaks. Ordered (11-1) diffraction peaks can be observed in the in-plane direction for blends with BTP-C9-N2F and BTP-C9-N4F as acceptors, which could be caused by the shortened alkyl substituents and the fluorine substituent in the end group.[47–49] A stronger π–π interaction can be observed in the out-of-plane direction, indicating a preferential face-on orientation, which could be beneficial for the charge transport between the anode and cathode of solar cell devices.[50,51] Moreover, the coexistence of face-on and edge-on orientations could facilitate the

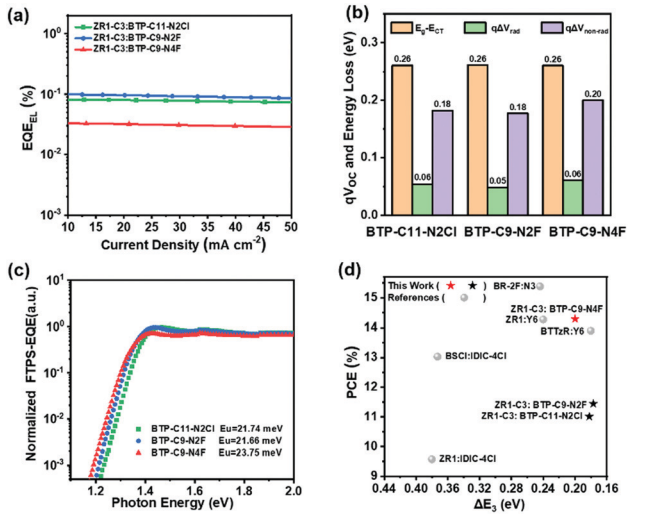

Fig. 5 (a) EL quantum efficiency of optimal blend films at different injected currents. (b) Graphically illustrating the detailed voltage loss of the OSCs with different acceptors. (c) FTPS-EQE of the three acceptors at the absorption onset and their calculated Urbach energies. (d) Recent studies on ASM-OSCs with low ΔE_3 and high PCE.

Table 2 Detailed V_{OC} loss based on BTP-C11-N2Cl, BTP-C9-N2F and BTP-C9-N4F with donor ZR1-C3

Acceptors	E_g [eV]	qV_{OC} [eV]	qV_{OC}^{SQ} [eV]	qV_{OC}^{rad} [eV]	qV_{loss} [eV]	ΔE_1 [eV]	ΔE_2 [eV]	ΔE_3 [eV]
BTP-C11-N2Cl	1.39	0.89	1.13	1.07	0.50	0.26	0.06	0.18
BTP-C9-N2F	1.39	0.90	1.13	1.08	0.49	0.26	0.05	0.18
BTP-C9-N4F	1.38	0.86	1.12	1.06	0.52	0.26	0.06	0.20

intermolecular charge transfer inside blends, giving high J_{SC} and FF, promoting a high PCE with low energy loss.

To further understand the reason for the various performances achieved by three similar acceptors, energy loss (E_{loss}) analysis was conducted. According to the Shockley–Queisser (SQ) limit model, the E_{loss} can be divided into the following:[38]

$$E_{loss} = E_g - qV_{OC} = (E_g - qV_{OC}^{SQ}) + (qV_{OC}^{SQ} - qV_{OC}^{rad}) + (qV_{OC}^{rad} - qV_{OC}) = \Delta E_1 + \Delta E_2 + \Delta E_3$$

where q is the elementary charge; E_g is the photovoltaic energy bandgap extracted from the derivation of the EQE curves,[52–54] V_{OC}^{SQ} is the maximum voltage based on the SQ limit and V_{OC}^{rad} is the open-circuit voltage when there is only radiative loss caused by the radiative recombination resulting from the absorption above the bandgap. All three blends exhibited a similar ΔE_1 value of 0.26 eV, ascribing from the similar E_g. ΔE_2 originates from the radiative recombination loss below the bandgap. A small ΔE_2 of 0.05–0.06 eV was obtained from the three blend films, which is almost negligible. ΔE_3 is the energy loss caused by nonradiative recombination and can be calculated by[29,55]

$$\Delta E_3 + q\Delta V_{non-rad} = qV_{OC}^{rad} - qV_{OC} = kT\ln(EQE_{EL})$$

where EQE_{EL} (Fig. 5a) represents the radiative quantum efficiency of the solar cell under dark current conditions and is calculated to be 8.00×10^{-4}, 9.57×10^{-4} and 3.15×10^{-4} for ZR1-C3:BTP-C11-N2Cl, ZR1-C3:BTP-C9-N2F and ZR1-C3:BTP-C9-N4F blends, respectively. The molecules with less substituted halogen atoms at the NINCN end group (*i.e.*, BTP-C11-N2Cl and BTP-C9-N2F) exhibited a higher EQE_{EL}, and thus lower nonradiative energy loss ΔE_3, which is in agreement with the E_{loss}, indicating the origin of the enhancement in V_{OC}. The high overall EQE_{EL} guaranteed a small nonradiative energy loss of less than 0.2 eV for all three blends, which is among the lowest in ASM-OPVs to the best of our knowledge. The estimated E_g, qV_{OC}^{SQ}, qV_{OC}^{rad}, qV_{loss}, ΔE_1, ΔE_2 and ΔE_3 are summarized in Table 2, and ΔE_1, ΔE_2 and ΔE_3 are plotted in Fig. 5b.

To gain more insight into the non-radiative voltage loss, the Urbach energy of pristine acceptors was measured by Fourier transform photocurrent spectroscopy external quantum efficiency (FTPS-EQE), as shown in Fig. 5c. A device structure of ITO/PEDOT:PSS/acceptor layer/PFN-Br/Ag was employed and the Urbach energy can be calculated by exponentially fitting of the tail of FTPS-EQE spectra following the equation[56]

$$E_U(E) = \left[\frac{d\ln(EQE)}{dE}\right]^{-1}$$

which quantifies the energy disorder of a system. Lower Urbach energies of less than 22 meV were obtained from BTP-C11-N2Cl and BTP-C9-N2F neat films compared with that of the BTP-C9-N4F pristine film, which is 23.75 meV. A lower Urbach energy indicates better intermolecular packing with less defects, and decreases the non-radiation recombination,[57] which is consistent with the energy loss analysis. Compared with polymer systems with PM6 as the donor,[23] ASM blends with ZR1-C3 as the donor have a smaller energy loss, mainly due to a lower ΔE_3, which further supports that small molecule donors may possess the potential to reach lower energy loss compared with polymers.

Conclusions

In summary, we designed and synthesized a series of small molecule donors ZR1-C2, ZR1-C3 and ZR1-C4 by varying the alkyne chain branching point. Small molecule acceptors BTP-C11-N4Cl, BTP-C9-N2F and BTP-C9-N4F were blended with ZR1-C3, giving a high V_{OC} with a small nonradiative energy loss $\leq$ 0.2 eV. Charge carrier mobilities, exciton dissociation efficiency and charge collection efficiency were measured and calculated, revealing good charge transport properties that support a high J_{SC}. Morphology characterization methods such as AFM, TEM and GIWAXS showed a fairly smooth surface with low RMS and interconnecting fibrous structures, indicating the good miscibility between the donor and acceptor, and the efficient charge transport channel that supports high J_{SC} and FF. A high PCE of 14.29% was achieved by the ZR1-C3:BTP-C9-N4F optimized device with low energy loss, which, to the best of our knowledge, is the highest PCE value among ASM-OSCs with a non-radiative voltage loss of $\leq$ 0.2 eV. The design of these kinds of small molecules is significant for the construction of high efficiency and low energy loss small molecule photovoltaics and shows the possibility of reaching a balance between the device performance and energy loss in ASM-OSCs.

Conflicts of interest

There are no conflicts to declare.

Acknowledgements

We acknowledge financial support provided by the National Natural Science Foundation of China (Grant No. 21822503 and 51973043) and the Youth Innovation Promotion Association, the Chinese Academy of Sciences.

Notes and references

1 L. Duan, H. Yi, Z. Wang, Y. Zhang, F. Haque, B. Sang, R. Deng and A. Uddin, Sustain, *Energy Fuels*, 2019, **3**, 2456–2463.
2 M. Kaltenbrunner, M. S. White, E. D. Glowacki, T. Sekitani, T. Someya, N. S. Sariciftci and S. Bauer, *Nat. Commun.*, 2012, **3**, 770.
3 R. Søndergaard, M. Hösel, D. Angmo, T. T. Larsen-Olsen and F. C. Krebs, *Mater. Today*, 2012, **15**, 36–49.
4 Y. Li, *Acc. Chem. Res.*, 2012, **45**, 723–733.
5 L. Lu, T. Zheng, Q. Wu, A. M. Schneider, D. Zhao and L. Yu, *Chem. Rev.*, 2015, **115**, 12666–12731.
6 G. Li, R. Zhu and Y. Yang, *Nat. Photonics*, 2012, **6**, 153–161.
7 K. Gao, S. B. Jo, X. Shi, L. Nian, M. Zhang, Y. Kan, F. Lin, B. Kan, B. Xu, Q. Rong, L. Shui, F. Liu, X. Peng, G. Zhou, Y. Cao and A. K. Jen, *Adv. Mater.*, 2019, **31**, 1807842.
8 Q. Liu, Y. Jiang, K. Jin, J. Qin, J. Xu, W. Li, J. Xiong, J. Liu, Z. Xiao, K. Sun, S. Yang, X. Zhang and L. Ding, *Sci. Bull.*, 2020, **65**, 272–275.
9 L. Zhan, S. Li, X. Xia, Y. Li, X. Lu, L. Zuo, M. Shi and H. Chen, *Adv. Mater.*, 2021, **33**, 2007231.
10 Y. Lin, J. Wang, Z. G. Zhang, H. Bai, Y. Li, D. Zhu and X. Zhan, *Adv. Mater.*, 2015, **27**, 1170–1174.
11 J. Zhang, H. S. Tan, X. Guo, A. Facchetti and H. Yan, *Nat. Photonics*, 2018, **3**, 720–731.
12 Y. Cui, H. Yao, J. Zhang, K. Xian, T. Zhang, L. Hong, Y. Wang, Y. Xu, K. Ma, C. An, C. He, Z. Wei, F. Gao and J. Hou, *Adv. Mater.*, 2020, **32**, 1908205.
13 C. Yan, S. Barlow, Z. Wang, H. Yan, A. K. Y. Jen, S. R. Marder and X. Zhan, *Nat. Rev. Mater.*, 2018, **3**, 18003.
14 H. Chen, D. Hu, Q. Yang, J. Gao, J. Fu, K. Yang, H. He, S. Chen, Z. Kan, T. Duan, C. Yang, J. Ouyang, Z. Xiao, K. Sun and S. Lu, *Joule*, 2019, **3**, 3034–3047.
15 S. D. Collins, N. A. Ran, M. C. Heiber and T.-Q. Nguyen, *Adv. Energy Mater.*, 2017, **7**, 1602242.
16 J. Ge, Q. Wei, R. Peng, E. Zhou, T. Yan, W. Song, W. Zhang, X. Zhang, S. Jiang and Z. Ge, *ACS Appl. Mater. Interfaces*, 2019, **11**, 44528–44535.
17 F. Pan, M. Luo, X. Liu, H. Jiang, Z. Wang, D. Yuan, Q. Wang, L. Qing, Z. Zhang, L. Zhang, Y. Zou and J. Chen, *J. Mater. Chem. A*, 2021, **9**, 7129–7136.
18 D. Hu, Q. Yang, H. Chen, F. Wobben, V. M. Le Corre, R. Singh, T. Liu, R. Ma, H. Tang, L. J. A. Koster, T. Duan, H. Yan, Z. Kan, Z. Xiao and S. Lu, *Energy Environ. Sci.*, 2020, **13**, 2134–2141.
19 X. Wang, J. Wang, J. Han, D. Huang, P. Wang, L. Zhou, C. Yang, X. Bao and R. Yang, *Nano Energy*, 2021, **81**, 2211–2855.
20 J. Ge, L. Xie, R. Peng, B. Fanady, J. Huang, W. Song, T. Yan, W. Zhang and Z. Ge, *Angew. Chem., Int. Ed.*, 2020, **59**, 2808–2815.
21 D. Hu, Q. Yang, Y. Zheng, H. Tang, S. Chung, R. Singh, J. Lv, J. Fu, Z. Kan, B. Qin, Q. Chen, Z. Liao, H. Chen, Z. Xiao, K. Sun and S. Lu, *Adv. Sci.*, 2021, **8**, 2004262.
22 L. Nian, Y. Kan, K. Gao, M. Zhang, N. Li, G. Zhou, S. B. Jo, X. Shi, F. Lin, Q. Rong, F. Liu, G. Zhou and A. K. Y. Jen, *Joule*, 2020, **4**, 2223–2236.
23 Y. Shi, J. Pan, J. Yu, J. Zhang, F. Gao, K. Lu and Z. Wei, *Sol. RRL*, 2021, **5**, 2100008.
24 Z. Zhang, Q. Wu, D. Deng, S. Wu, R. Sun, J. Min, J. Zhang and Z. Wei, *J. Mater. Chem. C*, 2020, **8**, 15385–15392.
25 Y. Zeng, D. Li, Z. Xiao, H. Wu, Z. Chen, T. Hao, S. Xiong, Z. Ma, H. Zhu, L. Ding and Q. Bao, *Adv. Funct. Mater.*, 2021, **11**, 2101338.
26 T. J. Wen, Z. X. Liu, Z. Chen, J. Zhou, Z. Shen, Y. Xiao, X. Lu, Z. Xie, H. Zhu, C. Z. Li and H. Chen, *Angew. Chem., Int. Ed.*, 2021, **60**, 12964–12970.
27 D. Qian, Z. Zheng, H. Yao, W. Tress, T. R. Hopper, S. Chen, S. Li, J. Liu, S. Chen, J. Zhang, X. K. Liu, B. Gao, L. Ouyang, Y. Jin, G. Pozina, I. A. Buyanova, W. M. Chen, O. Inganas, V. Coropceanu, J. L. Bredas, H. Yan, J. Hou, F. Zhang, A. A. Bakulin and F. Gao, *Nat. Mater.*, 2018, **17**, 703–709.
28 Y. Qin, S. Zhang, Y. Xu, L. Ye, Y. Wu, J. Kong, B. Xu, H. Yao, H. Ade and J. Hou, *Adv. Energy Mater.*, 2019, **9**, 1901823.
29 J. Liu, S. Chen, D. Qian, B. Gautam, G. Yang, J. Zhao, J. Bergqvist, F. Zhang, W. Ma, H. Ade, O. Inganäs, K. Gundogdu, F. Gao and H. Yan, *Nat. Energy*, 2016, **1**, 16089.
30 D. Baran, T. Kirchartz, S. Wheeler, S. Dimitrov, M. Abdelsamie, J. Gorman, R. S. Ashraf, S. Holliday, A. Wadsworth, N. Gasparini, P. Kaienburg, H. Yan, A. Amassian, C. J. Brabec, J. R. Durrant and I. McCulloch, *Energy Environ. Sci.*, 2016, **9**, 3783–3793.
31 R. Yu, G. Wu and Z. A. Tan, *J. Energy Chem.*, 2021, **61**, 29–46.
32 R. Zhou, Z. Jiang, C. Yang, J. Yu, J. Feng, M. A. Adil, D. Deng, W. Zou, J. Zhang, K. Lu, W. Ma, F. Gao and Z. Wei, *Nat. Commun.*, 2019, **10**, 5393.
33 R. Zhou, Z. Jiang, Y. Shi, Q. Wu, C. Yang, J. Zhang, K. Lu and Z. Wei, *Adv. Funct. Mater.*, 2020, **30**, 2005426.
34 W. Gao, X. Ma, Q. An, J. Gao, C. Zhong, F. Zhang and C. Yang, *J. Mater. Chem. A*, 2020, **8**, 14583–14591.
35 H. Feng, N. Qiu, X. Wang, Y. Wang, B. Kan, X. Wan, M. Zhang, A. Xia, C. Li, F. Liu, H. Zhang and Y. Chen, *Chem. Mater.*, 2017, **29**, 7908–7917.
36 R. Qin, D. Wang, G. Zhou, Z.-P. Yu, S. Li, Y. Li, Z.-X. Liu, H. Zhu, M. Shi, X. Lu, C.-Z. Li and H. Chen, *J. Mater. Chem. A*, 2019, **7**, 27632–27639.
37 T. Liu, X. Pan, X. Meng, Y. Liu, D. Wei, W. Ma, L. Huo, X. Sun, T. H. Lee, M. Huang, H. Choi, J. Y. Kim, W. C. Choy and Y. Sun, *Adv. Mater.*, 2017, **29**, 1604251.
38 J. Yao, T. Kirchartz, M. S. Vezie, M. A. Faist, W. Gong, Z. He, H. Wu, J. Troughton, T. Watson, D. Bryant and J. Nelson, *Phys. Rev. Appl.*, 2015, **4**, 014020.
39 J. Yuan, Y. Xu, G. Shi, X. Ling, L. Ying, F. Huang, T. H. Lee, H. Y. Woo, J. Y. Kim, Y. Cao and W. Ma, *J. Mater. Chem. A*, 2018, **6**, 10421–10432.
40 Q. Liang, J. Han, C. Song, X. Yu, D.-M. Smilgies, K. Zhao, J. Liu and Y. Han, *J. Mater. Chem. A*, 2018, **6**, 15610–15620.
41 B.-H. Jiang, C.-P. Chen, H.-T. Liang, R.-J. Jeng, W.-C. Chien and Y.-Y. Yu, *Dyes Pigm.*, 2020, **181**, 108613.
42 L. Ye, H. Hu, M. Ghasemi, T. Wang, B. A. Collins, J. H. Kim, K. Jiang, J. H. Carpenter, H. Li, Z. Li, T. McAfee, J. Zhao, X. Chen, J. L. Y. Lai, T. Ma, J. L. Bredas, H. Yan and H. Ade, *Nat. Mater.*, 2018, **17**, 253–260.
43 Z. Liu and N. Wang, *Dyes Pigm.*, 2021, **187**, 109111.

44 R. Zhou, C. Yang, W. Zou, M. Abdullah Adil, H. Li, M. Lv, Z. Huang, M. Lv, J. Zhang, K. Lu and Z. Wei, *J. Energy Chem.*, 2021, **52**, 228–233.
45 X. Yang, J. Loos, S. C. Veenstra, W. J. Verhees, M. M. Wienk, J. M. Kroon, M. A. Michels and R. A. Janssen, *Nano Lett.*, 2005, **5**, 579–583.
46 Q. An, J. Wang, W. Gao, X. Ma, Z. Hu, J. Gao, C. Xu, M. Hao, X. Zhang, C. Yang and F. Zhang, *Sci. Bull.*, 2020, **65**, 538–545.
47 D. Han, T. Kumari, S. Jung, Y. An and C. Yang, *Sol. RRL*, 2018, **2**, 1800009.
48 Y. Cho, T. H. Lee, S. Jeong, S. Y. Park, B. Lee, J. Y. Kim and C. Yang, *ACS Appl. Energy Mater.*, 2020, **3**, 7689–7698.
49 Y. Zhang, Y. Cho, J. Lee, J. Oh, S.-H. Kang, S. M. Lee, B. Lee, L. Zhong, B. Huang, S. Lee, J.-W. Lee, B. J. Kim, Y. Li and C. Yang, *J. Mater. Chem. A*, 2020, **8**, 13049–13058.
50 Y. Lin, F. Zhao, Q. He, L. Huo, Y. Wu, T. C. Parker, W. Ma, Y. Sun, C. Wang, D. Zhu, A. J. Heeger, S. R. Marder and X. Zhan, *J. Am. Chem. Soc.*, 2016, **138**, 4955–4961.
51 Y. Lin, Q. He, F. Zhao, L. Huo, J. Mai, X. Lu, C. J. Su, T. Li, J. Wang, J. Zhu, Y. Sun, C. Wang and X. Zhan, *J. Am. Chem. Soc.*, 2016, **138**, 2973–2976.
52 Y. Wang, D. Qian, Y. Cui, H. Zhang, J. Hou, K. Vandewal, T. Kirchartz and F. Gao, *Adv. Funct. Mater.*, 2018, **8** 1801352.
53 D. Veldman, S. C. J. Meskers and R. A. J. Janssen, *Adv. Funct. Mater.*, 2009, **19**, 1939–1948.
54 X. Liu, X. Du, J. Wang, C. Duan, X. Tang, T. Heumueller, G. Liu, Y. Li, Z. Wang, J. Wang, F. Liu, N. Li, C. J. Brabec, F. Huang and Y. Cao, *Adv. Energy Mater.*, 2018, **8**, 1801699.
55 K. Vandewal, K. Tvingstedt, A. Gadisa, O. Inganäs and J. V. Manca, *Phys. Rev. B: Condens. Matter Mater. Phys.*, 2010, **81**, 125204.
56 C. Kaiser, O. J. Sandberg, N. Zarrabi, W. Li, P. Meredith and A. Armin, *Nat. Commun.*, 2021, **12**, 3988.
57 Z. Zhang, Y. Li, G. Cai, Y. Zhang, X. Lu and Y. Lin, *J. Am. Chem. Soc.*, 2020, **142**, 18741–18745.

